J Seismol
https://doi.org/10.1007/s10950-020-09950-3

ORIGINAL ARTICLE

Seismic noise wavelet-based entropy in Southern California

Alexey Lyubushin

Received: 23 April 2020 / Accepted: 10 August 2020

Abstract Seismic noise properties in Southern California are considered. The initial data are continuous records of vertical oscillations with a sampling frequency of 1 Hz at 81 broadband stations for 12 years, 2008–2019. These data were converted to a time step of 1 min by calculating the average values in successive time intervals of 60 samples in length. The time series of low-frequency seismic noise with a time step of 1 min from each station was further converted to a sequence of daily values of the minimum normalized entropy of the distribution of the squared orthogonal wavelet coefficients. Since entropy estimates can be obtained from each station with a time step of 1 day, this makes it possible to construct a daily map of its changes in space. A general map of the distribution of entropy values is obtained by averaging daily maps. The main attention is paid to areas in which maximum entropy values are most often realized. These areas are identified by estimating the spatial probability density of the distribution of points at which a given number of maximum values are realized in each daily map. It has been shown that since 2012, the region of the most frequent realizations of entropy maxima is in direct contact with the epicenter of a strong earthquake on July 6, 2019, with magnitude 7.1. We consider the "secondary" entropy calculated for the probability densities of the distribution of the maximum values of the "primary" entropy of waveforms of seismic noise in a semi-annual moving time window. It is shown that the time intervals of increasing seismic activity correspond to a decrease in secondary entropy, which is interpreted as the concentration in the space of the distribution of the maxima of the primary noise entropy. Estimates of the change in the correlation coefficients between the daily values of the noise entropy in a semi-annual time window at network nodes of 12 reference points covering the region under study made it possible to study the spatiotemporal dynamics of strong correlations. The area of the future strong earthquake is characterized by high correlations of entropy values at the nearest reference points with other points.

Keywords Low-frequency seismic noise · Wavelets · Entropy · Earthquakes

1 Introduction

Seismic noise is a reflection of the inner life of the planet and is an important source of information that allows us to study processes in the lithosphere, including those that precede strong earthquakes (Lyubushin 2012, 2013, 2018a, 2018b). The total contribution of all weak earthquakes that occur daily, according to the Gutenberg-Richter recurrence law, is one to two orders of magnitude lower than the energy of constant seismic noise. Therefore, we can conclude that the main source of energy for the Earth's seismic background is not earthquakes, but cyclone movements in the atmosphere and the effect of ocean waves on the shelf and coast (Ardhuin et al. 2011; Aster et al. 2008; Friedrich et al. 1998; Grevemeyer et al. 2000; Kobayashi and Nishida 1998; Rhie and Romanowicz

A. Lyubushin (✉)
Institute of Physics of the Earth, Russian Academy of Sciences, Moscow, Russia
e-mail: lyubushin@yandex.ru

Published online: 21 August 2020

2004, 2006; Tanimoto 2001, 2005). Nevertheless, that the source of energy for low-frequency seismic noise is out of the Earth's crust (ocean and the atmosphere), the crust is a medium of seismic wave propagation. Thus, it is logical to assume that the processes inside the crust are reflected in changes in the statistical properties of seismic noise and the study of these properties allows us to determine the structural features of the crust (Berger et al. 2004; Fukao et al. 2010; Koper and de Foy 2008, Koper et al. 2010; Nishida et al. 2008, 2009; Stehly et al. 2006). In particular, variations in noise properties can be a source of information about changes in the Earth's crust that accompany the seismic process (Lyubushin 2010, 2014a, 2014b, 2015, 2017, 2020).

The article investigates the properties of the seismic noise wavelet-based entropy from continuous recordings of broadband seismic stations of 3 networks in Southern California for 12 years, 2008–2019. The main goal of the article is to identify areas with increased entropy of seismic noise and significant spatial correlations according to calculations in a moving time window, which is interpreted as a method for assessing short-term current seismic hazard.

2 Data

The data of the association of three broadband seismic regional networks in California were considered. The data are presented by the addresses:

http://ds.iris.edu/mda/AZ, http://ds.iris.edu/mda/BK, http://ds.iris.edu/mda/CI

They are provided by the operation of 81 stations in the studied rectangular region, shown in Fig. 1. For the analysis, a time interval of 12 years was selected, 2008–2019. Figure 1 shows the positions of 12 reference points, which will be used later for the analysis of spatial correlations of the entropy of seismic noise. In addition, stars indicate the epicenters of the two strongest seismic events in Southern California that occurred during the time interval 2008–2019. Data on seismic events were taken from the site https://earthquake.usgs.gov/earthquakes/search/ . For analysis, we selected those stations that have broadband sensors and vertical vibrations with a sampling frequency of 1 Hz.

Figure 2 explains why 2008 was chosen as the beginning of time interval for analyzing the data. The graph in Fig. 2 presents the daily numbers of operable seismic stations from 1990 up to the end of 2019.

From Fig. 2 we can notice that starting from 2008 the number of operable stations has no abrupt changes, which were observed earlier. The data of the vertical components were reduced to a time step of 1 min by calculating the average values in successive time intervals of 60 values in length.

Besides other purposes coming to 1-min time step provides avoiding from anthropogenic seismic noise, which is mainly concentrated within frequency band 1–10 Hz (Inbal et al. 2018).

3 Choosing set of reference points

We have chosen 12 reference points, which cover the region (Fig. 1). The number 12 was taken as the optimum number of clusters, which splits the "cloud" of seismic stations by *k*-means method. Let us split cloud of vectors of station positions $\vec{\zeta}$ into given probe number q of clusters using standard *k*-means cluster procedure (Duda et al. 2000). Let Γ_r, $r = 1, \ldots, q$ be clusters, $\vec{z}_r = \sum_{\vec{\zeta} \in \Gamma_r} \vec{\zeta} / n_r$ be vector of the center of cluster Γ_r, and n_r be a number of vectors within cluster Γ_r, $\sum_{r=1}^{q} n_r = N$. Vector $\vec{\zeta} \in \Gamma_r$ if the distance $|\vec{\zeta} - \vec{z}_r|$ is minimum among all positions of clusters' centers. *K*-means procedure minimizes sum

$$S\left(\vec{z}_1, \ldots, \vec{z}_q\right) = \sum_{r=1}^{q} \sum_{\vec{\zeta} \in \Gamma_r} \left|\vec{\zeta} - \vec{z}_r\right|^2 \to \min_{\vec{z}_1, \ldots, \vec{z}_q} \quad (1)$$

with respect to positions of clusters' centers $\vec{z}_r$. Let $J(q) = \min_{\vec{z}_1, \ldots, \vec{z}_q} S\left(\vec{z}_1, \ldots, \vec{z}_q\right)$. We try probe number of clusters within range $2 \le q \le 20$. The problem of selecting the best number of clusters q^* was solved from maximum of pseudo-*F*-statistics (Vogel and Wong 1979)

$$\mathrm{PFS}(q) = \sigma_1^2(q) / \sigma_0^2(q) \to \max_{2 \le q \le 20} \quad (2)$$

where

$$\sigma_0^2(q) = \frac{J(q)}{N-q}, \sigma_1^2(q) = \sum_{r=1}^{q} \frac{n_r}{N} \left|\vec{z}_r - \vec{z}_0\right|^2, \vec{z}_0 = \frac{1}{N} \sum_{t=1}^{N} \vec{\zeta} \quad (3)$$

Figure 3 presents the graph of pseudo-*F*-statistics, and we see that probe number of clusters 12 provides

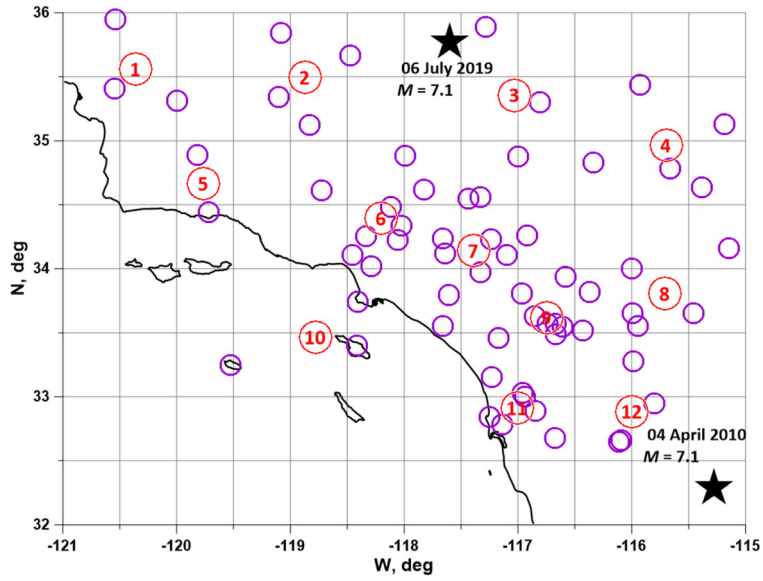

Fig. 1 Purple circles—positions of 81 seismic stations in Southern California, red numbered circles—positions of 12 reference points, and asterisks—epicenters of earthquakes, M ≥ 7

it maximum. That was the reason for selecting set of 12 reference points.

4 Seismic noise wavelet-based entropy

Let be $x(t)$ a finite sample of some random signal, $t = 1, \ldots, N$ be an index numbering consecutive samples (discrete time). We define the normalized entropy by the formula:

$$En = -\sum_{k=1}^{N} p_k \cdot \log(p_k)/\log(N), \quad p_k = c_k^2 / \sum_{j=1}^{N} c_j^2, \quad 0 \le En \le 1 \tag{4}$$

Here c_k, $k = 1, N$ are the coefficients of the orthogonal wavelet decomposition with some basis. The following 17 orthogonal Daubechies wavelets were used: 10 ordinary bases with minimal support with the number of vanishing moments from 1 to 10 and 7 so-called Daubechies symlets (Mallat 1999)), with the number of vanishing moments from 4 to 10. For each of the bases, the normalized entropy of the square distribution was calculated coefficients (4) and found a basis that provides a minimum value of (4). Note that due to the orthogonality of the wavelet transform, the sum of the squared coefficients is equal to the variance (energy) of the signal $x(t)$. Thus, quantity (4) calculates the entropy

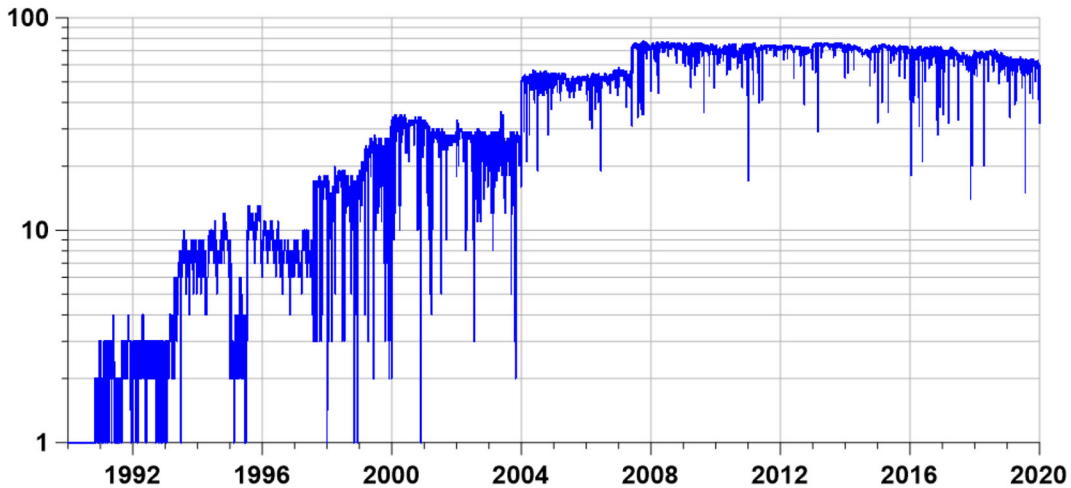

Fig. 2 Daily numbers of operable stations

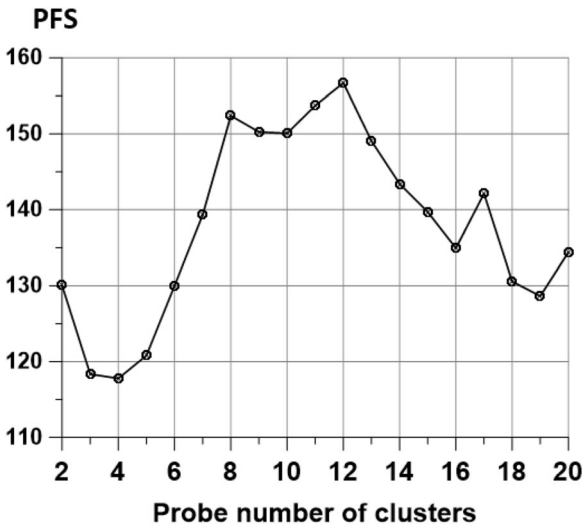

Fig. 3 Graph of pseudo-*F*-statistics which helps choosing the number of reference points

of the distribution of energy of oscillations at various frequency and time scales. Before calculating the normalized entropy (4), an operation was performed to eliminate the trend by an 8th order polynomial in order to get rid of deterministic trends caused by the influence of tidal and thermal deformations of the Earth's crust and to proceed to the study of noise characteristics. The order 8 of trend polynomials was chosen experimentally as minimum order which provides removing of deterministic low-frequency seismic waveforms components. The examples of waveforms before and after removing trends will be presented further on at Fig. 10 in the section where waveforms with high and low entropy values are compared. The entropy (4) was calculated after coming to 1-min time step and removing trends by polynomials of 8th order.

Entropy (4) by construction has much in common with multiscale entropy (Costa et al. 2003, 2005). It should also point out the related construction of entropy based on the use of the natural time approach (Sarlis et al. 2018; Varotsos et al. 2011).

Figure 4 shows a graph of daily median entropy values (4) calculated for all stations in the network. A periodic component with maximum entropy values in the winter period and minima in the summer season is visible. The most probable reason for the appearance of seasonal changes in the values of entropy is the different intensity of cyclonic activity in the atmosphere in winter and summer, which is the main source of energy of low-frequency seismic noise.

Having daily values of *En* from all operable seismic stations, it is possible to create maps of spatial distribution of this seismic noise statistics. For this purpose let us consider the regular grid of the size 60×60 nodes covering the rectangular domain with latitudes between 32 and 36°N and longitudes between 115 and 121°W (see Fig. 1). For each node of this grid the corresponding daily values of *En* are found, which are calculated as median for the values of five nearest to the node operable seismic stations. This simple procedure provides the sequence of daily maps. The averaged maps are created by averaging daily maps for all days between 2 given dates. The method of nearest neighbors provides a rather natural extrapolation of the used values into domains, which have no points of observations. Let us denote by $En_{ij}^{(t)}$ the entropy corresponding to the grid node (i,j) and to the daily time interval with number t. Each grid vector $En_{ij}^{(t)}$ could be regarded as "elementary" daily map. We can consider averaged map:

$$\overline{E}n_{ij}(t_0,t_1) = \sum_{t=t_0}^{t_1} En_{ij}^{(t)} / (t_1 - t_0 + 1) \qquad (5)$$

which corresponds to some intervals of time index t from minimum t_0 up to maximum t_1. Figure 5 presents the averaged map (5) for all available time indexes t covering all history of observations 2008–2019.

In Fig. 5, a region of lower entropy values is clearly distinguished, which corresponds to the Salton Sea geothermal field and Salton Buttes mud volcanoes complex, which is the site of moderate earthquakes associated with the geothermal system and movements along regional faults (Mangan et al. 2019). Volcanic tremors and the mutual movement of small blocks of the Earth's crust lead to the appearance of unsteady high-amplitude spikes in waveforms of low-frequency seismic noise, due to which entropy is greatly reduced.

5 Two-dimensional probability densities of maximum noise entropy values

Let us consider values of entropy as a function of 2D vectors of longitudes and latitudes $z_{ij} = (x_i, y_j)$ of nodes (i,j) explicitly: $En_{ij}^{(t)} \equiv En^{(t)}(z_{ij})$. For each daily "elementary map" with discrete time index t we will find coordinates $z_{mn}^{(t)} = \left(x_m^{(t)}, y_n^{(t)}\right)$ of the nodes where the entropy attain a given number n_m of maximum values with

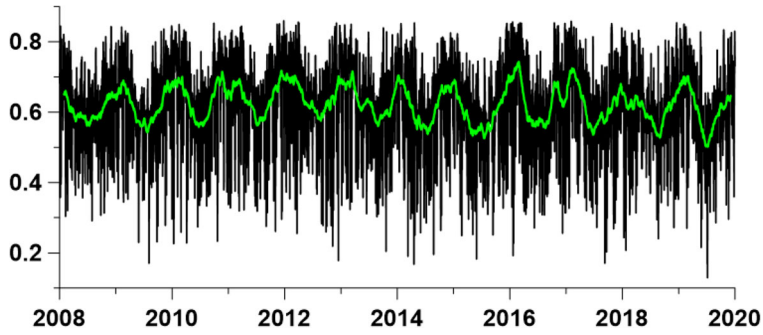

Fig. 4 Graph of daily median values of the minimum normalized entropy of seismic noise in Southern California. The green line shows the moving average in a window 57 days long

respect to all other nodes of the regular grid. Further on we will use $n_m = 10$ maximum values of entropy. The cloud of 2D vectors $z_{mn}^{(t)}$, which are regarded within some time interval $t \in [t_0, t_1]$ forms some random set. Let us estimate their 2D probability distribution function for each node z_{ij} of the regular grid. For this purpose, we will use Parzen–Rosenblatt estimate with Gaussian kernel function (Duda et al. 2000):

$$p(z_{ij}|t_0,t_1) = \frac{1}{2\pi n_m h^2 (t_1 - t_0 + 1)} \times \sum_{t=t_0}^{t_1} \sum_{mn} \exp\left(-\frac{\left|z_{ij} - z_{mn}^{(t)}\right|^2}{2h^2}\right) \quad (6)$$

Here h is the radius of kernel averaging (smoothing bandwidth); t_0, t_1 are integers indexes which numerate daily "elementary" maps. Thus, $(t_1 - t_0 + 1)$ is the number of 5-day maps within the considered time interval. We used the smoothing bandwidth $h = 0.2^\circ$. Figure 6 presents maps of probability density estimate (6) for time indexes t corresponding to 6 adjacent time fragments of the length 2 years.

Kernel estimates (6) of the probability densities of extreme values of statistics of random fluctuations of geophysical fields in a moving time window were used in Lyubushin (2019).

Low entropy values are due to the large number of spikes that arise due to the mutual movement of small blocks of the Earth's crust. High entropy values arise due to the small number of high-amplitude variations of seismic noise, which can be associated with increased consolidation of small blocks of the Earth's crust. The formation of a large consolidated block contributes to energy storage and, therefore, increases seismic hazard. Thus, the increased values of the probability density of the distribution distinguish those areas of the region under study that the maxima of entropy are most often realized and which are suspicious from the point of view of increased seismic hazard.

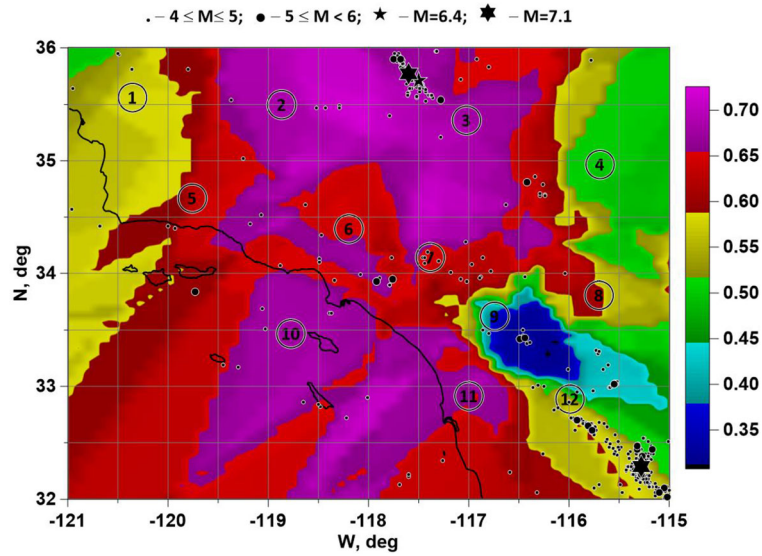

Fig. 5 Averaged map for distribution of the values of the minimum normalized entropy of seismic noise for the entire observation period, 2008–2019; numbered circles—positions of 12 reference points. Epicenters of earthquakes in different ranges of magnitudes for $M \geq 4$ are shown. For $M \geq 6$, one event $M = 6.4$ and two events $M = 7.1$ occurred

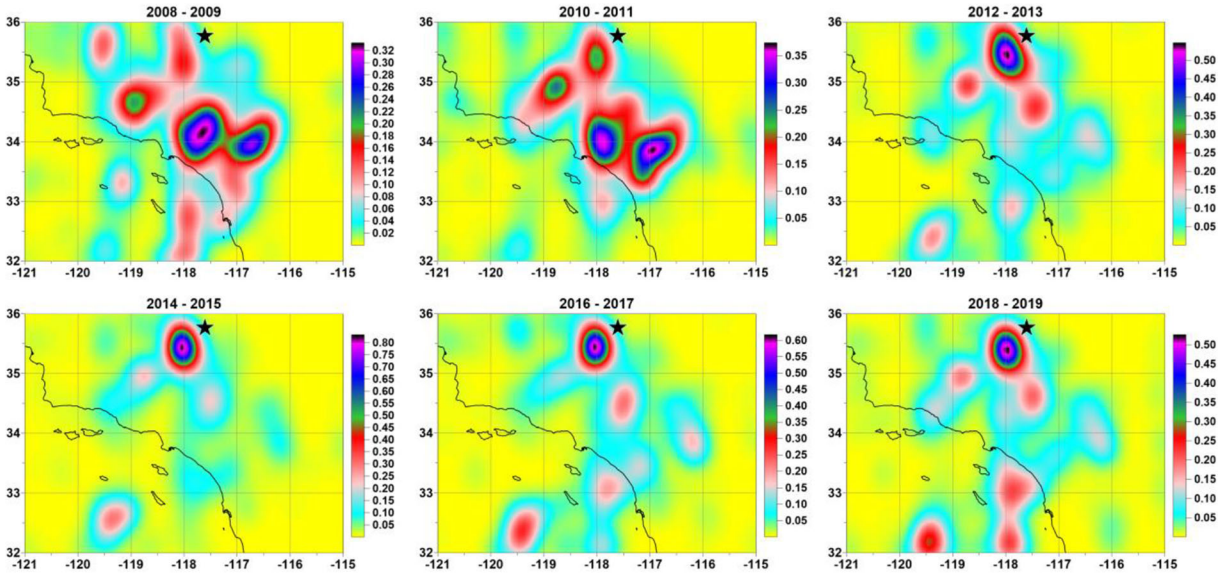

Fig. 6 Averaged maps of 2-dimensional distribution probability densities of 10 maximum values of the minimum normalized entropy of seismic noise for 4 adjacent 2-year time intervals. The asterisk shows the epicenter of the earthquake on July 6, 2019, $M = 7.1$

6 Secondary entropy

If we take the moving time window with some rather short length, then the sequence of plots, which are similar to Fig. 6, will present a time-spatial dynamics of seismic noise field of entropy. In connection with this possibility, it is of interest to calculate some measure that would characterize the degree of diversity of the location of spots of high probability density of maximum entropy values in space. As such a measure, it is natural to use Shannon informational entropy (Gray 1990) of 2-dimensional probability density:

$$En(t_0, t_1) = -\int_S p(z|t_0, t_1) \cdot \log(p(z, y|t_0, t_1))\, dz / \log(|S|) \tag{7}$$

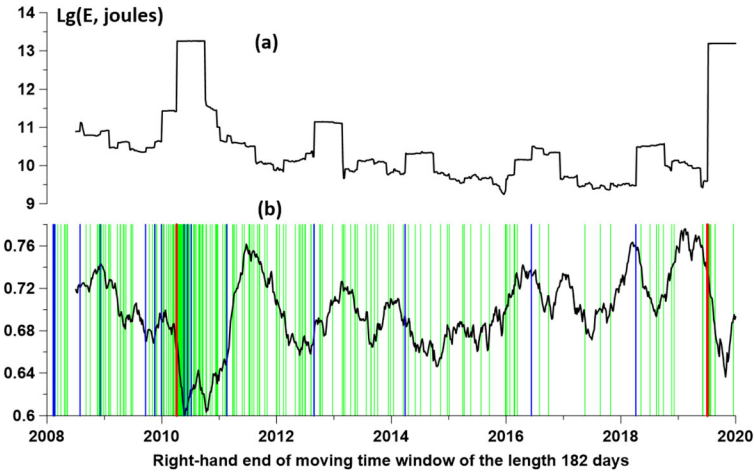

Fig. 7 **a** is a graph of the logarithms of the energy released in the sequence of seismic events in a moving time window of 182 days in length with an offset of 5 days; **b** is a graph of the "secondary" entropy of 2-dimensional probability distribution densities of 10 maximum values of the "primary" minimum normalized entropy of seismic noise in a moving time window of 182 days in length. The vertical lines indicate the moments of time of earthquakes in different ranges of magnitudes: green lines—$4 \le M \le 5$; blue lines—$5 < M \le 6$; red lines—$6 < M$

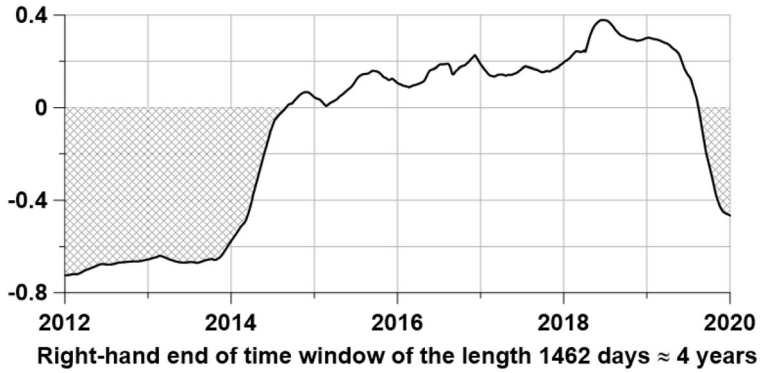

Fig. 8 Graph of the correlation coefficient between the logarithms of the released seismic energy and the values of the "secondary" entropy calculated in the "short" windows 182 days long, in the "long" time window 257 values long (1462 days or about 4 years)

Let us call the entropy defined by formula (7) as "secondary" entropy, i.e., entropy of probability distribution function of maximum values of "primary" seismic noise entropy, which is defined by formula (4). Here S is the 2D region under the investigation, and $|S|$ is its area. According to (7) the value of entropy is normalized $0 \le En \le 1$. Let us consider the sequence of time windows of length 182 days (half year) taken with mutual shift of 5 days and estimate the entropy (7) of 2D density functions (6) for each time window. Figure 7 b presents a graph of normalized entropy (7) for such sequence of time windows in dependence on the right-hand end of time windows.

When choosing a "long" window, it should be borne in mind that the values of the secondary entropy of seismic noise are obtained by evaluations in "short" time windows of 182 days in length, taken with an offset of 5 days. Thus, if we take adjacent L values of secondary entropy, then the dimension length of the "long" time window will be equal to $N = 182 + (L-1) \cdot 5$ days. When choosing $L = 257$ the value of the $N = 1462$ days. The number of days in 4 adjacent years is 1461, taking into account the fact that in each interval of 4 years, 1 year is a leap year. Therefore, the choice $L = 257$ provides a time window of 4 years with great accuracy.

Figure 8 shows a graph of the correlation coefficient between the secondary entropy of seismic noise and the logarithm of the energy released by the sequence of earthquakes in Southern California in a moving time window with a length of 257 adjacent values (approximately 4 years) with a minimum shift of one value (5 days).

A comparison of the graphs in Figs. 7 and 8 shows that an increase in seismic activity corresponds to a decrease in secondary entropy. This is expressed in negative values of the correlation coefficient between the logarithms of the released seismic energy and secondary entropy in Fig. 8 at the beginning and end of the considered time interval of 2008–2019. The decrease in secondary entropy, according to the meaning of this quantity, can be interpreted as the concentration in space of "spots" corresponding to the maxima of the primary noise entropy. And since the concentration of increased values of primary entropy is associated with an increase in seismic hazard, those areas where entropy takes on maximum values most often are distinguished as areas of increased danger.

7 Spatial correlations

For a detailed analysis of the temporal changes in spatial correlations between the primary entropy values, we consider a network of 12 reference points whose positions are defined as the centers of the clusters of positions of seismic stations determined by the k-means method. The positions of these 12 reference points are shown in Figs. 1 and 5.

Figure 9 shows graphs of daily values of primary entropy at 12 reference points, calculated as medians of values at the 5 nearest operational stations. They can be considered as samples of typical entropy behavior in the vicinity of reference points, covering the entire region under study quite densely. Attention should be paid to the values of entropy at the point number 9, which is located in the region of reduced entropy on the map in Fig. 5—it can be seen how abnormally small these values are compared with the time series for other reference points. In addition, the behavior of entropy for reference point 9 shows an interval of particularly low values in the interval 2013–2018, the existence of which could not be attributed to any manifestations of seismicity in the vicinity of this point. Most likely, such an abnormally low value of entropy is associated with the activation of processes in Salton Buttes volcanoes

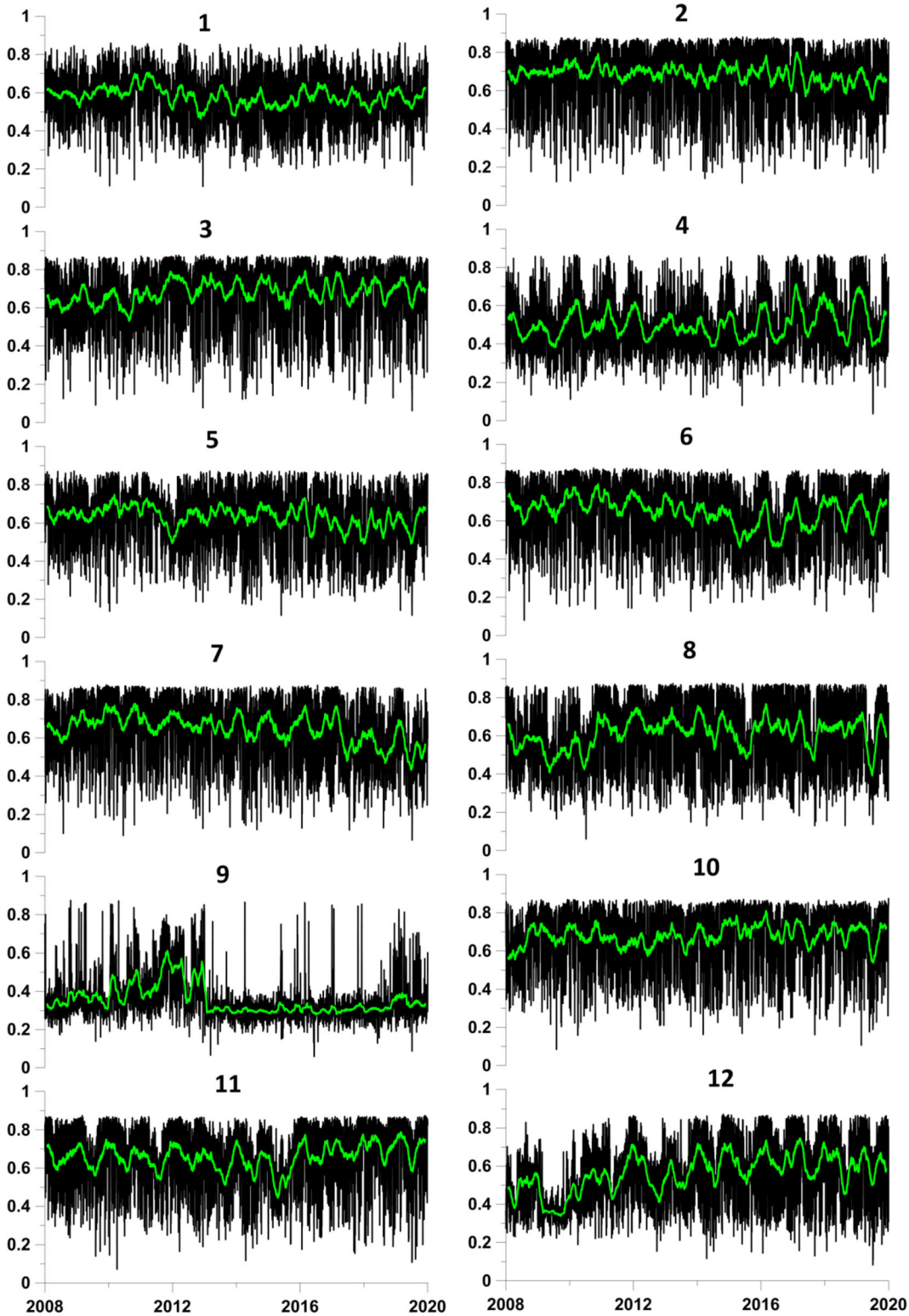

Fig. 9 Graphs of daily median values of the minimum normalized entropy of seismic noise calculated for 12 reference points (see Fig. 1) from 5 nearest operational stations. The green lines show the moving averages in a 57-day window

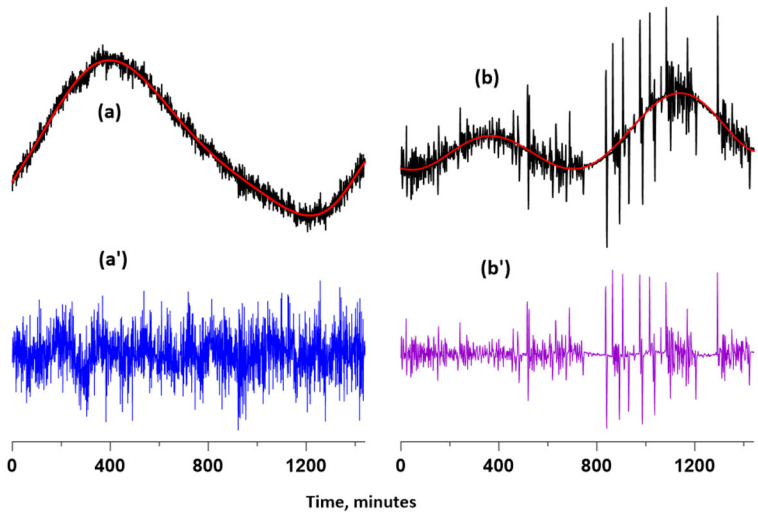

Fig. 10 Examples of daily waveforms of low-frequency seismic noise after coming to a time step of 1 min before ((a) and (b)) and after ((a′) and (b′)) removing trends by an 8th order polynomial (red lines at (a) and (b)); (a, a′) ARV station with coordinates (-118.83 ° W, 35.127 ° N), located near reference point 2; (b, b′) COR station with coordinates (-116.74 ° W, 33.57 ° N), located near reference point 9. A question arises whether it is possible to use polynomial of lower order for detrending. Order 8 was taken with some margin in order to effectively remove the trend from a waveform characterized by a complex trend, for example, in Fig. 10 (b). To remove the trend in Fig. 10 (a), one could do with a lower order polynomial, for example 4. But the presence of 2 oscillations during the day in Fig. 10 (b) requires the 8th order. Removing trends was performed within each daily time window independently from detrending in other time windows. A rather high 8th order of polynomial provides removing influence of temperature variations and tides within a rather short daily time window

(Mangan et al. 2019). Figure 10 shows the plots of the daily waveforms of low-frequency seismic noise at two stations located in the vicinity of reference point 2 and point 9 before and after the trend has been removed by an 8th order polynomial. A comparison of Fig. 10 (a′) and (b′) visually illustrates the reason for the decrease in noise entropy due to the presence of high-amplitude emissions in graph 10(b').

A set of 12 time series, together with the coordinates of the reference points, allows us to estimate the temporal change in the spatial parameters of the correlation of entropy values in the region. For this purpose, we

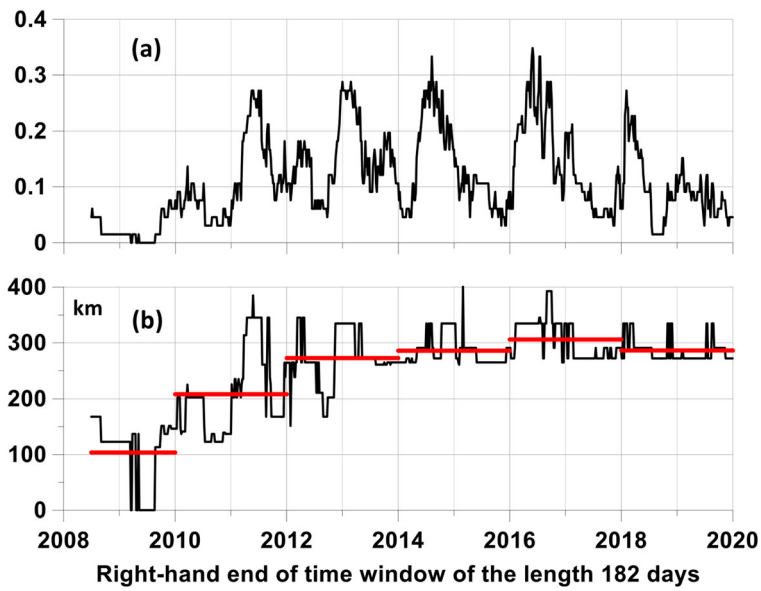

Fig. 11 **a** The proportion of pairs of reference points between which an absolute correlation occurred, exceeding the threshold of 0.7 in a moving time window of 182 days in length with an offset of 5 days. **b** The maximum value of the distances between the reference points for which the module of the correlation coefficients in a moving time window of 182 days in length exceeded the threshold of 0.7. The horizontal red lines show the average values of the maximum distances for time marks of the right-hand ends of the moving windows in 6 adjacent intervals

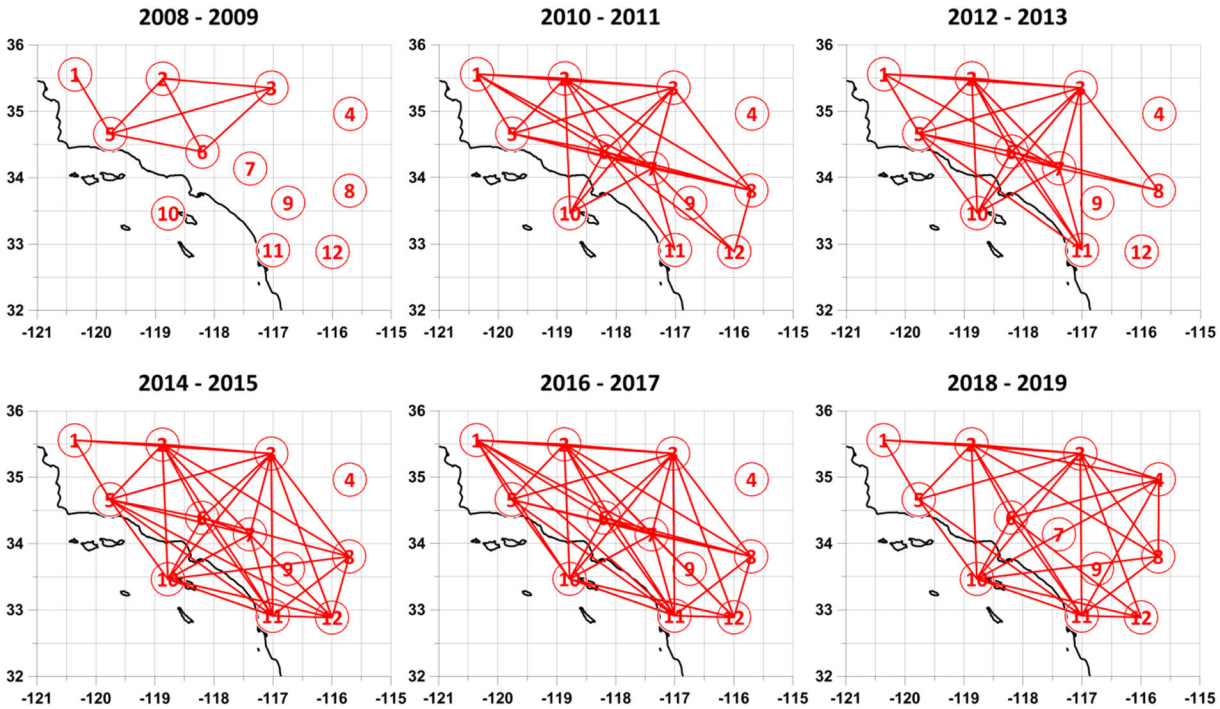

Fig. 12 The red lines show the pairs of 12 reference points between which an absolute correlation occurred, exceeding the threshold of 0.7 in "short" sliding time windows 182 days long with a shift of 5 days for 6 adjacent time intervals of the time marks of the right-hand ends of the windows

consider a moving time window of 182 days in length with an offset of 5 days and in each window we calculate the absolute values of all pairwise correlations between the increments of time series shown in Fig. 9. With a total of 12 such values the number of pairwise correlations will be 66. Of these pairwise correlations, we choose only those values that exceed the threshold of 0.7; that is, we consider only fairly strong correlations between the values at the reference points.

Figure 11 a shows a graph of the change in the ratio of the number of strong correlations exceeding the threshold of 0.7 to the total number of all pairwise correlations, that is, to 66. This ratio can be considered as a measure of the connectedness of values at different

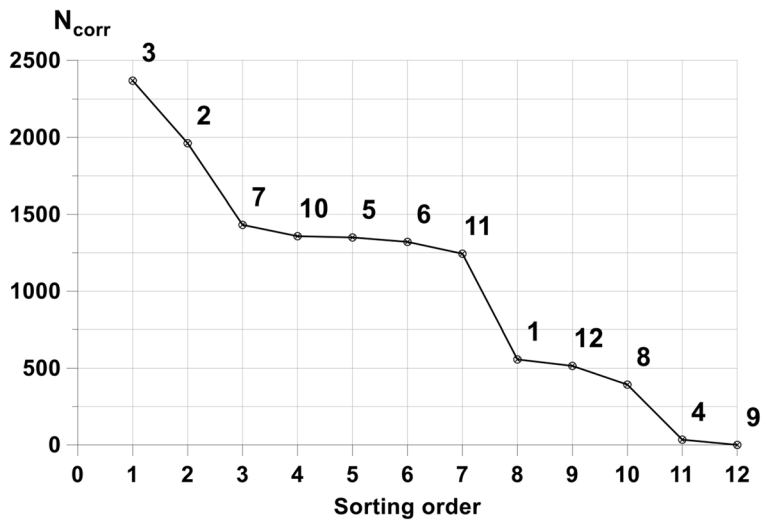

Fig. 13 The total numbers of strong correlations N_{corr} within the windows 182 days long for each of the 12 reference points, sorted in descending order

Table 1 The total number of strong correlations N_{corr} that arose in the windows with a length of 182 days for each of the 12 reference points. The reference points with the greatest number of such correlations are highlighted in red; the control points with the least number of strong correlations are highlighted in blue

#	1	2	3	4	5	6	7	8	9	10	11	12
N_{corr}	557	1962	2370	34	1350	1321	1432	393	0	1358	1244	515

nodes of the network of control points. Such a measure was considered, for example, in Laib et al. (2018).

The data at the reference points make it possible to estimate the spatial characteristics of strong correlations, for example, the maximum distance between the reference points for which the correlation coefficient inside the half-year moving time window between the entropy values moduli exceeded the threshold 0.7. A graph of this dependence is shown in Fig. 11b. It shows that the maximum linear size of strong correlations grows from zero in 2009 to 250–300 km in 2012. Note that 2012 is the beginning of the time when a spot of high values of the two-dimensional probability density of the distribution of maxima of the primary entropy of seismic noise in space in the immediate vicinity of the epicenter of the earthquake on July 6, 2019, $M = 7.1$, was formed (see Fig. 6). The red lines in Fig. 11b show the changes in the average values of the maximum distances.

Another possibility to visualize spatial correlations is to construct a graph of the correlation connectivity of reference points. Consider 6 adjacent time intervals of the values of the timestamps of the right-hand ends of the moving time windows 182 days in length, taken with an offset of 5 days. We connect by a straight line those pairs of reference points for which the correlation coefficient between the values of the primary noise entropy in at least one of these windows in absolute value exceeded the threshold of 0.7. The result of these operations is shown in Fig. 12.

The sequence of graphs in Fig. 12 helps to understand how the "involvement" of various reference points in spatial correlations changes. For example, the peripheral point with number 4 established strong correlations only in the last interval of time marks 2018–2019. As for the reference point 9, it generally never establishes strong correlations with any other point, despite the fact that it is in their environment.

To quantify the "strength" of spatial correlations, we calculate the total occurrence numbers of strong correlations between pairs of reference points in a moving time window of 182 days in length and sort them in descending order. Sorted values depending on the number in descending order are shown in Fig. 13.

The graph in Fig. 13 allows you to divide the reference points into 3 groups—"strong" correlations, "medium," and "weak." This separation is presented in Table 1.

Two reference points with numbers 2 and 3 are distinguished by their high values of the total numbers of strong correlations. Other points are divided into 2 groups: with low total numbers of correlations—these are numbers 1, 4, 8, 9, and 12 and with average values—points with numbers 5, 6, 7, 10, and 11. Note that points 6, 7, and 9, despite their middle position in the cloud of reference points, they do not establish maximum numbers of strong correlations with their neighbors, as one might assume from the simplest hypothesis that the closer the reference points, the more likely the variation in the values of entropy for them is more correlated. As already noted, point 9 does not enter into strong correlations with any other point at all. For points 2 and 3, despite their peripheral position, the establishment of strong correlations with a large number of other reference points is characteristic. This suggests that the establishment of strong spatial correlations occurs nonlinearly and with the long-range effect. Note that points 2 and 3 are located near the epicenter of the strongest seismic event on July 6, 2019, $M = 7.1$. This allows us to conclude that the preparation of a strong earthquake is accompanied by the establishment of strong correlations in the variations in the entropy of seismic noise in the vicinity of a future event.

In connection with this hypothesis, the question naturally arises, why there are no such strong correlations before the first strong event on April 4, 2010, $M = 7.1$ for the nearest reference point with number 12? Moreover, as follows from Table 1, this reference point is characterized by a low total number of strong correlations. Apparently, this is due to the peculiarity of the geological structure of Southern California—the presence of sources of powerful interference in the form of chaotic sequences of spikes in the records of the low-

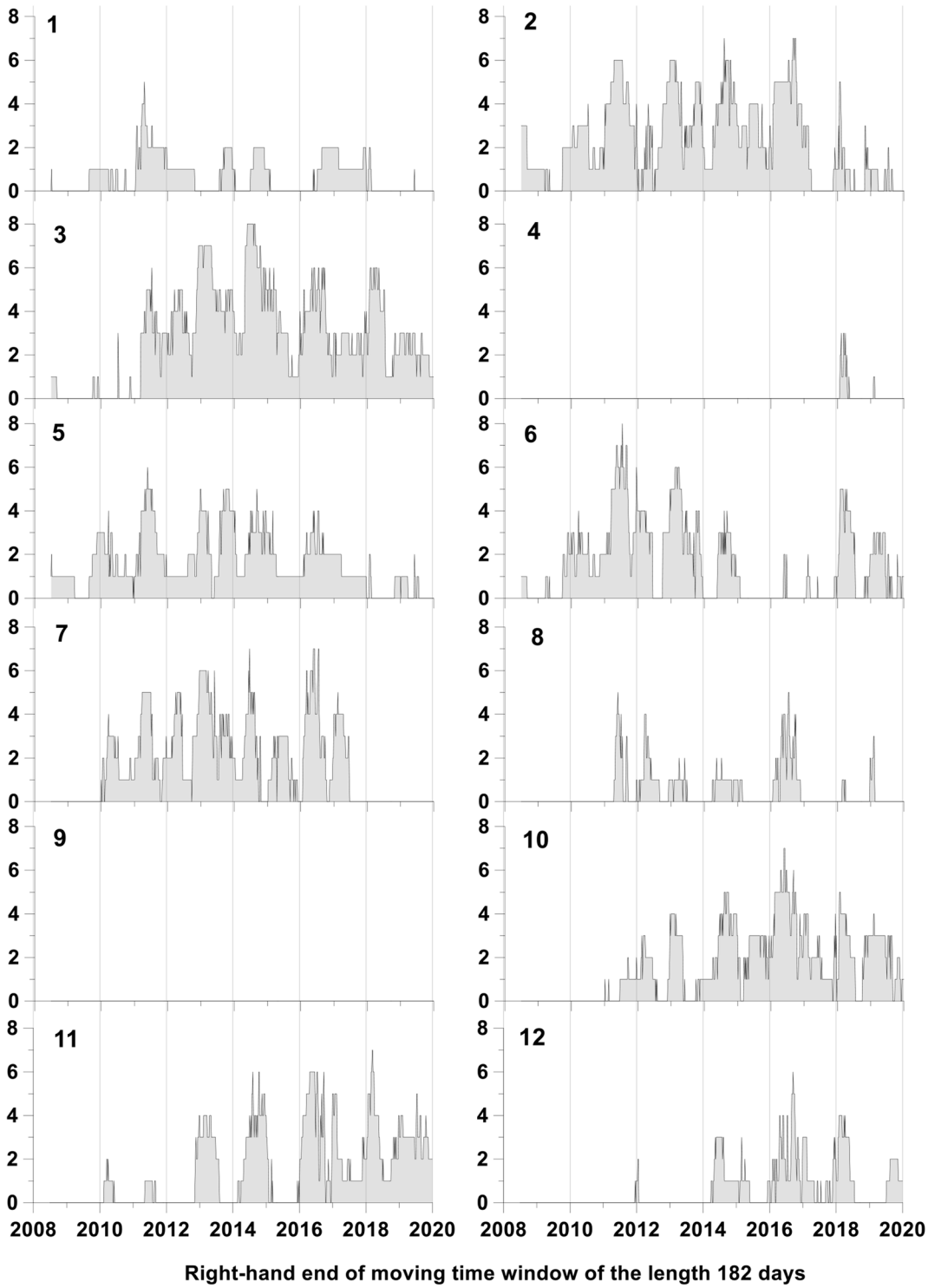

Fig. 14 Graphs of the numbers of strong correlations that arose for each of 12 reference points with some other reference point in a sliding window 182 days long with an offset of 5 days

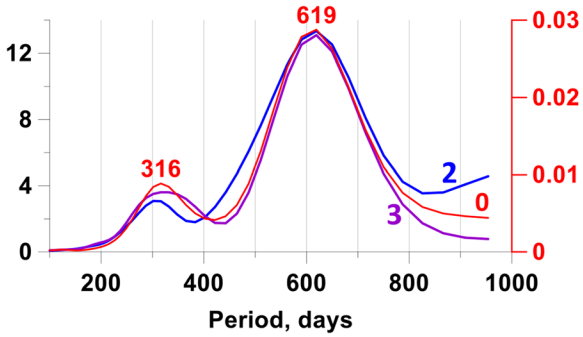

Fig. 15 Graphics of Morlet wavelet spectra; blue and magenta lines (labels "2" and "3")—for sequences of strong correlation numbers for reference points 2 and 3 (see Fig. 14) in a sliding time window 182 days long with an offset of 5 days, the left *Y* axis is used; the red line (label "0")—for the sequence of the share of pairs of reference points between which an absolute correlation has occurred, exceeding the threshold of 0.7 in a moving time window 182 days long (see Fig. 11a), the right *Y* axis is used

frequency seismic noise from the nearby mud volcanoes Salton Buttes (Mangan et al. 2019), which can be seen when comparing waveforms in Fig. 10. For the same reason, in Fig. 6, the vicinity of the epicenter of the first strong earthquake, shown in Fig. 1, does not contain increased values of the probability density of the spatial distribution of the maximum values of the noise entropy.

The data of Table 1 can be "expanded" in time and presented as graphs of the numbers of strong correlations for each of the control points that arose in a sliding time window 182 days in length with an offset of 5 days. These graphs are shown in Fig. 14.

It is interesting to note that in the variations of the numbers of strong correlations for points 2 and 3, one can see the periodicity of the same nature as in Fig. 11a. We calculate the periods of variations of these quantities using the continuous Morlet wavelet transform (Mallat 1999). We denote by $y(s)$ the dependence of a particular quantity on time (the position of the right end of the time window) s and calculate the Morlet wavelet transform

$$c(t,a) = \frac{1}{\sqrt{a}} \int_{-\infty}^{+\infty} y(s) \cdot \psi\left(\frac{s-t}{a}\right) ds, \quad a > 0, \quad \psi(t) = \frac{1}{\pi^{1/4}} \exp\left(-t^2/2 - i\pi t\right) \tag{8}$$

The values of $|c(t,a)|^2$ could be interpreted as the energy of oscillation of the signal $y(s)$ at the vicinity of time moment t with a period a. Wavelet-based Morlet spectrum is calculated as period-dependent mean values of $|c(t,a)|^2$ with respect to all time moments t. Figure 15 presents graphs of Morlet spectra, and it is obvious that all of them have common strong peaks at the periods 619 days (which is near 1.7 years) and 316 days.

8 Conclusion

A new method has been developed for analyzing the spatial and temporal properties of long-term continuous records of seismic background noise in seismically active areas, based on the calculation of the minimum normalized entropy of the distribution of the squares of the orthogonal wavelet coefficients of noise waveforms. The method includes estimating in a moving time window the probability densities of the maximum entropy values and strong spatial correlations between the entropy variations in the vicinity of a given set of reference points covering the region under study.

The method is applied to the analysis of seismic noise records in Southern California for 12 years, 2008–2019, on a network of 81 broadband seismic stations. The time interval 2009–2012 was found for the intensive growth of the linear size of strong spatial correlations for entropy values from zero to 250–300 km, after which the earthquake focus on July 6, 2019, M = 7.1 began to form. The preparation of this seismic event is manifested in the appearance of a stable spot of increased probability density values of the spatial distribution of the maximum values of the seismic noise entropy in the immediate vicinity of the source. In addition, the preparation of a strong earthquake is accompanied by the establishment of strong spatial correlations in the entropy variations of seismic noise in the vicinity of a future event, as well as the occurrence of periodic fluctuations in the characteristics associated with the spatial radius of strong entropy correlations with a period of about 1.7 years.

Our hypothesis consists in correlation between high values of entropy *En* and growth of seismic danger. A possible physical interpretation of ability of high values of *En* extract seismically dangerous regions is the consequence of consolidation of small blocks of the Earth's crust into the large one before the strong earthquake. Consolidation implies that seismic noise does not include spikes, which are connected with mutual movements of small blocks. The absence of irregular spikes in the noise follows increasing of entropy *En*.

It should be noted that the paper does not pretend to solve the problem of earthquake prediction in all its aspects. The goal of the paper is to show that a rather simply calculated property of low-frequency seismic noise (wavelet-based entropy) possesses ability to sense changes in the Earth's crust before strong earthquake for a rather long time interval before the event.

Funding information The research was supported by the Russian Foundation for Basic Research, Grant No. 18-05-00133, project "Estimation of fluctuations of seismic hazard on the basis of complex analysis of the Earth's ambient noise."

References

Ardhuin F, Stutzmann E, Schimmel M, Mangeney A (2011) Ocean wave sources of seismic noise. J Geophys Res 116: C09004

Aster R, McNamara D, Bromirski P (2008) Multidecadal climate induced variability in microseisms. Seismol Res Lett 79:194–202

Berger J., Davis P. and Ekstrom G., Ambient earth noise: a survey of the global seismographic network, J Geophys Res, 109 2004, B11307

Costa M, Peng C-K, Goldberger AL, Hausdorf JM (2003) Multiscale entropy analysis of human gait dynamics. Physica A 330(2003):53–60

Costa M, Goldberger AL, Peng C-K (2005) Multiscale entropy analysis of biological signals. Phys Rev E 71(2005):021906

Duda R.O., Hart P.E. and Stork D.G., Pattern Classification, 2000, Wiley-Interscience Publication, New York, Chichester, Brisbane, Singapore, Toronto

Friedrich A, Krüger F, Klinge K (1998) Ocean-generated microseismic noise located with the Gräfenberg array. J Seismol 2(1):47–64

Fukao YK, Nishida K, Kobayashi N (2010) Seafloor topography, ocean infragravity waves, and background love and Rayleigh waves. J Geophys Res 115:B04302

Gray RM (1990) Entropy and information theory. Springer-Verlag, New York, NY

Grevemeyer I, Herber R, Essen H-H (2000) Microseismological evidence for a changing wave climate in the northeast Atlantic Ocean. Nature 408:349–352

Inbal A, Cristea-Platon T, Ampuero JP, Hillers G, Agnew D, Hough SE (2018) Sources of long-range anthropogenic noise in Southern California and implications for tectonic tremor detection. Bull Seismol Soc Am 108(6):3511–3527. https://doi.org/10.1785/0120180130

Kobayashi N, Nishida K (1998) Continuous excitation of planetary free oscillations by atmospheric disturbances. Nature. 395:357–360

Koper KD, de Foy B (2008) Seasonal anisotropy in short-period seismic noise recorded in South Asia. Bull Seismol Soc Am 98:3033–3045

Koper KD, Seats K, Benz H (April 2010) On the composition of Earth's short-period seismic noise field. Bull Seismol Soc Am 100(2):606–617

Laib M, Telesca L, Kanevski M (2018) Long-range fluctuations and multifractality in connectivity density time series of a wind speed monitoring network. Chaos 28:033108 (2018). https://doi.org/10.1063/1.5022737

Lyubushin, A. (2010) Multifractal parameters of low-frequency microseisms, in synchronization and triggering: from fracture to earthquake processes, de Rubeis, V. et al., Eds., GeoPlanet: Earth and Planetary Sciences 1, Berlin: Springer, 2010, Chapter 15, pp.253–272. https://doi.org/10.1007/978-3-642-12300-9_15

Lyubushin A (2012) Prognostic properties of low-frequency seismic noise. Nat Sci 4(8A):659–666. https://doi.org/10.4236/ns.2012.428087

Lyubushin A (2013) How soon would the next mega-earthquake occur in Japan. Nat. Sci 5, A1(8):1–7. https://doi.org/10.4236/ns.2013.58A1001

Lyubushin AA (2014a) Dynamic estimate of seismic danger based on multifractal properties of low-frequency seismic noise. Nat Hazards 70(1):471–483. https://doi.org/10.1007/s11069-013-0823-7

Lyubushin AA (2014b) Analysis of coherence in global seismic noise for 1997–2012. Izv Phys Solid Earth 50(3):325–333. https://doi.org/10.1134/S1069351314030069

Lyubushin AA (2015) Wavelet-based coherence measures of global seismic noise properties, *J.* Seismol. 19(2):329–340. https://doi.org/10.1007/s10950-014-9468-6

Lyubushin AA (2017) Long-range coherence between seismic noise properties in Japan and California before and after Tohoku mega-earthquake. Acta Geodaetica et Geophysica 52:467–478. https://doi.org/10.1007/s40328-016-0181-5

Lyubushin A. (2018a) Synchronization of geophysical fields fluctuations, in Complexity of seismic time series: measurement and applications, Chelidze, T., Telesca, L., and Vallianatos, F., Eds., Amsterdam: Elsevier, 2018, Chapter 6, pp. 161–197. https://doi.org/10.1016/B978-0-12-813138-1.00006-7

Lyubushin AA (2018b) Cyclic properties of seismic noise and the problem of predictability of the strongest earthquakes in Japanese Islands. Izvestiya, Atmospheric and Oceanic Physics 54(10):1460–1469. https://doi.org/10.1134/S0001433818100067

Lyubushin, A. (2019) Field of coherence of GPS-measured earth tremors. GPS solutions (2019) 23:120. First Online: 27 September 2019. https://doi.org/10.1007/s10291-019-0909-0

Lyubushin AA (2020) Trends of global seismic noise properties in connection to irregularity of Earth's rotation //. Pure and Applied Geophysics 177(2):621–636. https://doi.org/10.1007/s00024-019-02331-z

Mallat S (1999) A wavelet tour of signal processing, Second edn. Academic Press, San Diego, London, Boston, New York, Sydney, Tokyo, Toronto

Mangan M, Ball J, Wood N, Jones JL, Peters J, Abdollahian N, Dinitz L, Blankenheim S, Fenton J, Pridmore C (2019) California's exposure to volcanic hazards (ver. 1.1, December 2019). US Geol Surv Sci Investig Rep 2018–5159:49 p. https://doi.org/10.3133/sir20185159

Nishida K, Kawakatsu H, Fukao Y, Obara K (2008) Background love and Rayleigh waves simultaneously generated at the Pacific Ocean floors. Geophys Res Lett 35:L16307

Nishida K, Montagner J, Kawakatsu H (2009) Global surface wave tomography using seismic hum. Science 326(5949): 112

Rhie J, Romanowicz B (2004) Excitation of Earth's continuous free oscillations by atmosphere-ocean-seafloor coupling. Nature 2004(431):552–554

Rhie J, Romanowicz B (2006) A study of the relation between ocean storms and the Earth's hum. Geochem Geophys Geosyst 7(10). https://doi.org/10.1029/2006GC001274

Sarlis NV, Skordas ES, Mintzelas A, Papadopoulou KA (2018) Micro-scale, mid-scale, and macro-scale in global seismicity identified by empirical mode decomposition and their multifractal characteristics. Sci Rep 8:9206. https://doi.org/10.1038/s41598-018-27567-y

Stehly L, Campillo M, Shapiro NM (2006) A study of the seismic noise from its long-range correlation properties. J Geophys Res 111:B10306

Tanimoto T (2001) Continuous free oscillations: atmosphere-solid earth coupling. Annu Rev Earth Planet Sci 29:563–584

Tanimoto T (2005) The oceanic excitation hypothesis for the continuous oscillations of the Earth. Geophys J Int 160: 276–288

Varotsos P.A., Sarlis N.V. and Skordas E.S. Natural Time analysis: the new view of time. Precursory seismic electric signals, earthquakes and other complex time series, 2011, Springer-Verlag Berlin Heidelberg, 449 p. https://doi.org/10.1007/978-3-642-16449-1

Vogel MA, Wong AKC (1979 Mar) PFS clustering method. IEEE Trans Pattern Anal Mach Intell 1(3):237–245. https://doi.org/10.1109/tpami.1979.4766919 https://pubmed.ncbi.nlm.nih.gov/21868854/